High-performance screen-printable pastes for HJT cells

Stefan Körner & **Markus Eberstein**, Fraunhofer IKTS, Dresden, Germany

ABSTRACT

A highly promising concept for future solar cells is the heterojunction (HJT) architecture; according to the ITRPV roadmap 2016, the market share for HJT solar cells will increase to 10% by 2026. Over this timescale, stabilized cell efficiency will increase to 24%, which is the second-highest predicted efficiency after back-contact cells with n-type mono-Si. Moreover, metallization of HJT cells offers the advantage of using low-temperature steps, which reduces energy consumption and hence production costs. However, attaining the predicted goals requires a further improvement in the performance of metallization pastes in terms of process ability, conductivity, and contact resistance to the indium tin oxide (ITO) layer. Today's paste systems pose difficulties in handling during processing, especially with regard to the storage conditions. In the study reported in this paper, new metallization pastes for HJT solar cells are examined. These new pastes demonstrate excellent electrical performance using an infrared radiation-based curing profile, with efficiencies reaching 21.7%. Along with an additional gain in electrical characteristics, the standard deviation is decreased compared with conventional convection curing. The electrical performance of the new paste is similar to (or even better than) that of currently available reference metallization pastes, while a significantly easier handling and processing behaviour is observed. Using the contemporary generations of new pastes with bimodal silver mixture, the sheet resistance is decreased to 2.7mΩ/sq.

Introduction

The 2016 international technology roadmap for photovoltaics forecasts that the market share for silicon heterojunction (HJT) solar cells will see an increase of up to 10% by the year 2026; over this timescale, HJT cell efficiency is expected to increase to 24% [1]. This is the second-highest predicted efficiency after back-contact cells with n-type mono-Si.

> "The development of high-conductance systems that can be cured at temperatures lower than the required 200°C is a new challenge for paste manufacturers."

The HJT cell architecture includes two temperature-sensitive layers: 1) an intrinsic amorphous silicon for passivation of the base; and 2) a boron-doped amorphous layer as the emitter, obtained by plasma-enhanced chemical vapour deposition (PECVD). These two layers limit the maximum process temperature to 200°C in all subsequent process steps. As the top layer, an indium tin oxide layer (ITO) is deposited as transparent conductive oxide (TCO); this acts additionally as an anti-reflection coating and provides conductivity in the top layer, which decreases the contact resistance between the front-side metallization and the solar cell. As regards the metallization grid on top, the development of high-conductance systems that can be cured at temperatures lower than the required 200°C is a new challenge for paste manufacturers.

In the study reported here, the development of front-side metallization pastes for low-temperature applications was investigated. For low-temperature curable binders, different polymers were evaluated with regard to solubility in various solvents, rheological properties and curing conditions. Silver was added to the organic vehicle as a functional phase in the preparation of the pastes; the amount of silver was systematically varied, and the influence on the electrical properties was investigated. Solar cells were fabricated with these pastes and characterized. Additionally, nanoparticles and low melting point alloys (LMPAs) were examined as paste additions. The curing was carried out on a production scale in a new belt furnace, which provided heat transfer either by convection or by infrared in an air or a nitrogen atmosphere.

Polymer	Type	Glass transition [°C]	Melting point [°C]
A	Epoxy	110	>200
B	Epoxy	130	>200
C	Vinyl	68	135–210

Table 1. Types of polymer used in the study and selected thermal properties.

Solvent	Polarity	Boiling point [°C]
I	++	<100
II	0	>150
III	++	<100
IV	–	>200
V	+	>200
VI	0	>200
VII	– –	<100

Table 2. Polarities and boiling points of the different solvents used in the study.

Experiments

Organic vehicle preparation

For the preparation of the organic vehicle (or *binder*), different polymers were selected because of their thermal properties, such as glass transition and melting point (Table 1). The polymers were then dissolved in various solvents. The polarity of the solvents was varied (Table 2) in order to influence the solubility of the polymers and the binder properties, such as viscosity and curing conditions.

All polymer–solvent combinations were treated in the same way. A mixture of polymer and solvent was prepared and stirred with a magnetic stirrer; the solubility was evaluated after 1, 12 and 24 hours of stirring. Binders with fully dissolved polymer were thermally treated for 10 minutes at 150, 180, 200 and 240°C in order to determine the optimal curing conditions.

Paste production

After the preparation of the organic vehicle, the pastes were created. For this, two binders were chosen and mixed with a flaky silver powder with a particle size of less than 10µm. The powder was added gradually, and after each powder addition the paste was mixed in a centrifugal mixer (Speedmixer DAC150 FVZ). Homogenization using a three-roll mill was then performed. The solids content was varied systematically, and an attempt was made to maximize the content in order to lower the resistance in the final layer. During the curing process, the mass loss was determined so that the evaporation rate of the solvent could be controlled.

In the case of the paste preparation using the LMPA to reduce the amount of silver, a powder with a melting point of 138°C was chosen. The LMPA powder was treated with different organic reduction agents before paste preparation; this inhibited the oxidation of the non-noble powder during the curing of the final paste.

Besides the LMPA, silver nanoparticles were added to the paste; these nanoparticles were suspended in solvent V. The polymer was then added, in an appropriate fraction, to the suspension. Following the preparation of the nanoparticle pre-paste, the flaky silver powder was added.

All pastes were subsequently printed on alumina ceramic as the test substrate, and cured using different time–temperature regimes; electrical characterization was then performed. Additionally, field emission scanning electron microscopy (FESEM) images of cross sections of the chosen pastes were taken, and the relationship of conductivity with structural properties was determined.

Solar cell production

To test paste 7 on the solar cells, ten wafers (Meyer Burger Germany) were printed and cured. For comparison purposes, a state-of-the-art commercial paste was printed on ten wafers as well. The commercial pastes must be stored in a freezer at –20°C, whereas the IKTS paste can be stored in a conventional fridge at 7°C. Next, the wafers were split into two groups: five wafers of each paste were cured for 15 minutes at 200°C with convection heat transfer, and the other five wafers of each paste were cured using the same conditions but with IR heat transfer. All wafers were then electrically characterized using a GridTouch system.

Results and discussion

Organic vehicle

In contrast to conventional high-temperature metallization paste, the polymer remains in the film after thermal processing. In consequence, the polymer in an organic vehicle for low-temperature curable paste fulfils two tasks: 1) it adjusts the viscosity of the binder, which acts as a screen-printing medium; and 2) it facilitates the adhesion between the metal particles of the paste, as well as the adhesion to the surface of the wafer. With these functions in mind, it is important to create a binder system that can provide a high solids content, with a functional phase on the one hand, and excellent screen printability on the other.

Three polymers – A, B and C – were dissolved in the various solvents with different polarity and boiling point properties (Table 2). The first property influences the solubility of the polymer, while the second determines the screen printability. If the boiling point is too low, the paste will dry on the screen, whereas if the boiling point is too high, it will take too long for complete evaporation of the solvent during thermal processing. Table 4 gives an overview of suitable polymer–solvent combinations based

Paste	Organic vehicle [polymer/solvent]	Solids content in paste [%]		
		Silver	LMPA	Nano silver
1	A/V	64.1		
2	A/V	73.6		
3	A/V	77.6		
4	B/V	78.8		
5	B/V	80.2		
6	C/V	84.6		
7	C/V	86		
8	C/V	57.3	28.7	
9	C/V			66
10	C/V	37.2		37.2

Table 3. Paste compositions.

Solvent	Polymer		
	A	B	C
I	++	++	++
II	+	++	+
III	++	++	++
IV	–	0	–
V	+	0	+
VI	–	– –	++
VII	– –	– –	– –

Table 4. Solubility ratings of the polymers used in different solvents for this study.

on an evaluation of the solubility of the polymer in the solvent.

The solubility ratings of the investigated polymers illustrate that with increasing polarity of the solvent, the polymer can be dissolved completely. When less solvent or a non-polarized solvent is used, the solubility decreases and the polymer is not dissolved completely or is simply swollen. With the use of solvent VII (which is the most unipolar solvent), the polymer remained unchanged; after this pre-test, solvent VII was not pursued any further in this study.

After testing the solubility of the solvent, the curing conditions were determined. For this, a small amount of organic vehicle was provided on aluminium plates and cured in a box oven at different temperatures for 10 minutes. Fig. 1 shows the appearance of the cured organic vehicle prepared in the case of polymer B and solvents I to VI. For all curing conditions, a solid transparent film can be obtained; however, its colour ranges from colourless to amber. The latter indicates the first signs of degradation of the polymer, which can be caused either by exceeding a certain thermal budget or by reactions between solvent and polymer. Curing the polymer alone without any solvent will result in a colourless layer. In general, discolouring increases with increasing temperature: all solvent–polymer combinations, apart from solvents II and V, begin to discolour at 180°C. For solvents II and V, discolouring starts at the lowest temperature and increases with the thermal budget; in these cases it is concluded that there is a negative interaction between the solvents and the polymer.

When the highest curing temperature of 240°C is used, the thermal degradation for all solvents can be evidenced by the dark appearance of the samples. This temperature was chosen despite the maximum process temperature allowed by the HJT wafer, in order to determine if any effects of polymer degradation could be seen using this simple set-up.

The images for polymer A are not shown here; degradation effects cannot be seen because of the initial reddish colour of the polymer. The use of polymer C results in colourless layers, which did not show any negative influences from temperature or from solvent–polymer interactions. With this in mind, and taking into account the boiling points of the solvents, further experiments were performed just using solvent V. When solvents with boiling points below 100°C are used, this will probably result in fast-drying pastes which would be difficult to screen print. With the solvents II, IV and VI, which have the highest boiling points, it is possible that evaporation of the solvent will take too long and thus the pastes would not be a practical solution. Solvent V, however, should be a good compromise between solubility and curing conditions.

Paste characterization

The electrical conductivity of a polymer–silver composite depends on the solids content of silver in the cured layer. If the silver content is high enough, the conductivity in the dried layer is provided by percolation between the metal particles. Assuming a density of the organic vehicle of roughly 1g/cm^3, the critical silver content for percolation to occur between the particles is in the range 20–30vol% (72–82wt%) [2]. With this in mind, the paste was dried in order to increase the solids content, but still maintain its screen-printability. (See Table 3 for the composition of the pastes tested.)

Fig. 2 depicts the sheet resistances of the cured layers for pastes 1–7 as a function of curing temperature (black bar = 150°C, red bar = 200°C). Pastes 1–3 with polymer A demonstrate that a paste-curing temperature of 200°C reduces the resistivity of the final layer. For paste 1 the difference in resistance for the two temperatures is 18Ω/sq.; in contrast, for pastes 2 and 3 the difference is less than 60mΩ/sq. When

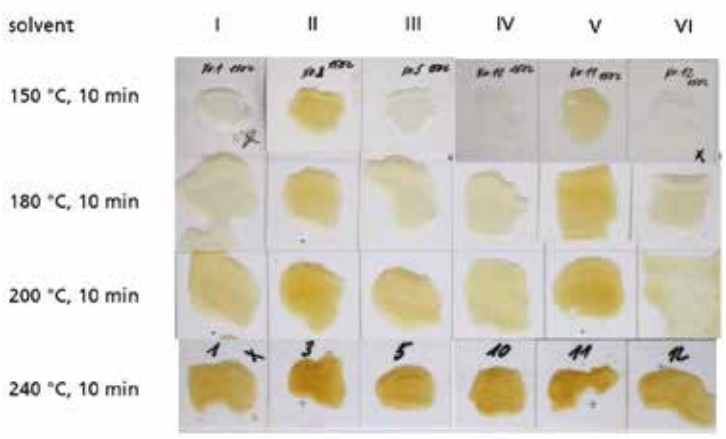

Figure 1. Images of polymer B dissolved in solvents I–VI and cured for 10 minutes at 150, 180, 200 and 240°C.

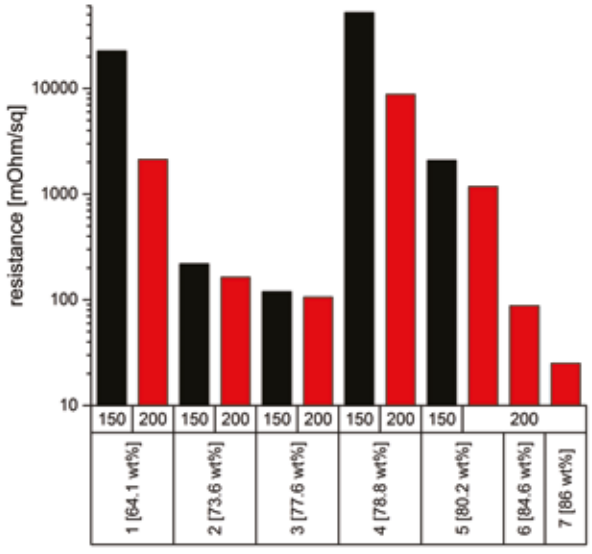

Figure 2. Sheet resistance of the cured layer as a function of paste composition and curing temperature (black bar = 150°C; red bar = 200°C). (The curing time was 10 minutes in all cases.)

the solids content is increased from 64.1wt% (paste 1) to 77.6wt% (paste 3), the resistance falls by approximately 2,000mΩ/sq. at 200°C. The corresponding difference for pastes 2 and 3 is of the order of 60mΩ/sq.

Increasing the amount of silver in the paste system increases the probability of creating percolation paths, and therefore of decreasing the resistance. However, a further increase in solids content was not possible with polymer A, and so the polymer matrix was changed to polymer B. Because of the change in polymer, it now became possible to increase the wt% of silver to 80.2.

The influence of temperature is similar to that for polymer A: with increasing temperature, the resistance decreases. At the same time, a higher temperature results in complete evaporation of the solvent used during organic vehicle preparation. With this in mind, it is reasonable to expect that somewhat better layer formation, especially the creation of percolation paths, could occur. Because of the higher temperature, the vapour pressure of the solvent is higher, and hence the rate of evaporation is increased. Earlier release of the solvent means that the particle arrangement in the polymer (which has not yet fully cross-linked) can happen more easily: more percolation paths are created and the resistance drops. The antagonist to this mechanism is the kinetics of the cross-linking of the polymer chains. If the cross-linking velocity is high, then the polymer hardens and consequently the solvent cannot evaporate completely. Residual solvent can increase the resistance in the final layer; moreover, the arrangement of the silver particles is hindered by the rapid cross-linking polymer matrix, which becomes very stiff and does not soften during the curing. The cross-linking for polymer B occurs somewhat faster than for polymer A, resulting in the higher resistances for paste 5 with 80.2wt% silver than for paste 3 with 77.6wt% silver.

> "Residual solvent can increase the resistance in the final layer."

In contrast, polymer C in the pastes 6 and 7 used in this study did not cross-link during curing; therefore, the solvent can evaporate completely and the silver particle arrangement can occur. By providing an optimal viscosity for paste preparation it is also possible to increase the solids content further in comparison to the pastes with other polymer matrices; when the silver content is maximized, it is possible to decrease the resistance to 25.1mΩ/sq. As regards the results for the other pastes, only the high temperature was chosen for curing in order to obtain the lowest possible resistance.

Fig. 3 shows FESEM images of cross sections of paste 3 (left) and paste 7 (right). For paste 3, the brightest regions are the silver particles, the black areas are the polymer, and the medium grey indicates inorganic inclusions from the polymer matrix (both types of particle are indicated by arrows in the figure). Between the silver particles there are black areas roughly 5µm in diameter; these are accumulations of polymer, and represent areas that are not fully homogenized with the other paste components. The image for paste 3 also shows particles that are medium grey in colour and have a diameter of around 4µm; energy dispersive X-ray (EDX) measurements were performed on these particles, and they were determined to be inorganic inclusions from the polymer.

To verify that these particles do not originate from paste preparation, the original polymer was investigated; the particles were also present in the original polymer. The commercial polymer is red, and so the conclusion is that these inorganic particles are the pigment for colouring the polymer. The cross-sectional image for paste 3 provides explanations for both the low silver content and the relatively high resistance of 106mΩ/sq. As a result of the inhomogeneous mixing of silver and polymer, the solids content is limited; additionally, these areas and

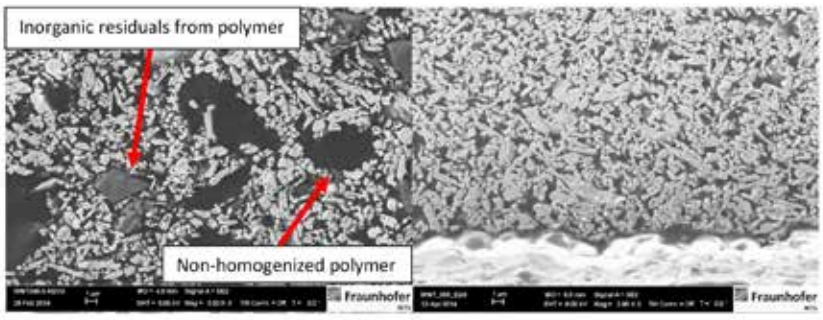

Figure 3. FESEM images of cross sections of paste 3 (polymer A; left hand side) and paste 7 (polymer C; right). Both pastes were printed on alumina for characterization and cured for 10 minutes at 200°C. (Images taken at 3,000× magnification.)

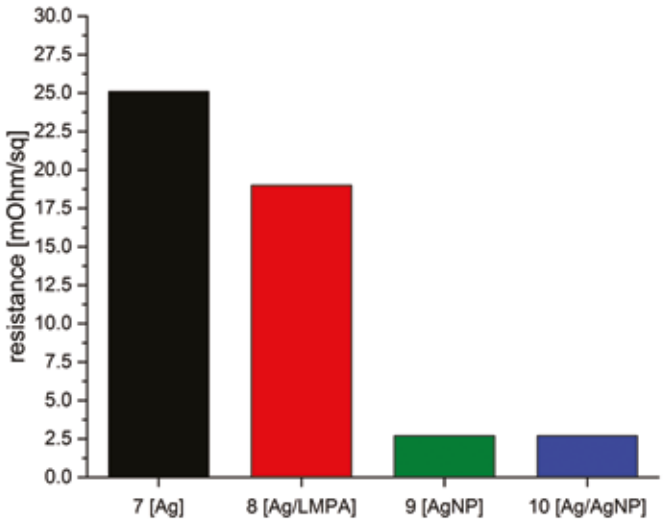

Figure 4. Sheet resistances of pastes 7–10 vs. their functional phases. All pastes were cured for 10 minutes at 200°C.

the inorganic particles are insulators and therefore increase the resistance of the cured layer.

The cross section for paste 7 (Fig. 3, right) shows a homogeneous distribution of the silver particles. The bright layer at the bottom of the image is the alumina substrate. In the paste layer itself, there are no areas of non-dispersed polymer or inorganic particles. The silver particles are close together, and there do not appear to be any insulating areas, despite the thin polymer layers between the silver particles. The probability of creating percolation paths, and hence decreasing the resistance, is high.

Another approach for decreasing the resistance by increasing the probability of conductive paths is the addition of an LMPA, which is a metal alloy with a melting point below 200°C. In most compounds of this type, the main metal is a non-noble one, and oxidation during heating is an issue. To prevent oxidation, the particles are coated with a reducing agent and then added to the metallization paste. With the controlled melting of the LMPA, conductivity is generated not just through the percolation paths between the silver, but also through the connection of the silver particles in the paste. A second effect is the decrease in cost because of the reduced amount of silver in the paste.

Yet another possibility for decreasing the resistance is to use bimodal silver powder mixtures. With these, there is an increase in packing density and thus in the number of connection points between the silver particles. If the particles are small enough, a second effect can occur: sintering can be induced because of the reduction in sintering temperature as a result of the phenomenon of melting point reduction.

Fig. 4 shows the sheet resistances of pastes 7–10 vs. their functional phases. Paste 7 (black) contains only micron-scale silver powder, providing conductivity simply by percolation paths. Paste 8 (red) includes as an additive an LMPA, which melts during curing. Because of this melting process, the silver particles are connected with each other. The conductivity in this case is provided both by percolation paths and by the silver particles connected during the melting phase. With the use of an LMPA, the resistance can be reduced from 25.1mΩ/sq. (paste 7) to 19.0mΩ/sq. (paste 8). Additionally the silver content can be lowered by one-third, which also decreases the cost of the paste.

Pastes 9 and 10, both of which contain silver nanoparticles, yield even lower resistances. Paste 9 (green) contains only nanoparticles in the metallization phase, whereas paste 10 (blue) contains a mixture of micron-scale and nano silver powder. Paste 9 delivers a sheet resistance of 2.7mΩ/sq., which is around one-tenth of that for micron-scale silver powder (paste 7). A mixture of small and large particles, as used in paste 10, can produce a similar resistance of 2.7mΩ/sq. In comparison to paste 9, however, only half of the functional phase for paste 10 consists of the cost-intensive nanoparticles. For both pastes, the silver content can be reduced by 11.6wt% compared with paste 7.

FESEM images of cross sections of pastes 7–10 are shown in Fig. 5. (Paste 7 is shown again for comparison purposes.) Paste 8 (Fig. 5, top right) contains two kinds of material: small particles of silver, and large particles of LMPA. The black areas indicate the polymer matrix. The areas without LMPA are comparable to those for paste 7 without additives (Fig. 5, top left). The LMPA particles are larger than the silver particles by a factor of ten. After curing, the surface is rough and the insides of the LMPA particles are bloated; this indicates partial melting of the particles, which results in a local melding of silver and LMPA. Controlled melting is necessary in order to prevent damage to the polymer matrix. If the LMPA is completely melted in an uncontrolled fashion, the polymer dissolves and disintegrates in the liquid metal phase, resulting in low adhesion to the substrate, as well as low adhesion of the particles to each other.

In paste 9 (Fig. 5, bottom left), the silver particles are dispersed homogeneously in the polymer matrix (black areas). For better visualization of the connections between the particles, this image has been taken at a higher magnification. The particle size is well below 500nm; with this, an initial sintering process can be provided, which results in sinter necks between the particles. This clearly results in a reduction in resistance to 2.7mΩ/sq.

Similar results can be obtained using a mixture of micron-scale and nano silver powder, as in paste 10 (bottom right). The nanoparticles are sintered together, resulting in the creation of sinter necks. Additionally, the nanoparticles are sintered with the micron-scale particles and connect them with each other. In this way, the quantity of expensive nanoparticles can be reduced without a loss in performance.

Solar cell production

Paste 7 was used to print the front-side metallization of some MeyerBurger HJT solar cells. For comparison purposes, a state-of-the-art commercially available paste for solar cell metallization was also used. To demonstrate the influence of oven atmosphere, both pastes were cured using the same profile (10 minutes at 200°C), but with different systems of

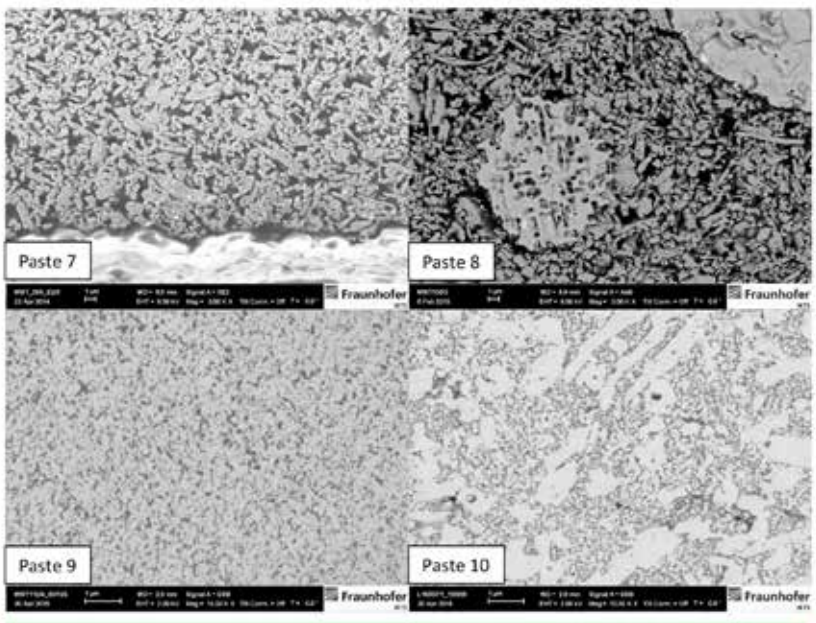

Figure 5. FESEM images of cross sections of pastes 7–10. Each paste was printed on alumina for characterization and cured for 10 minutes at 200°C. (Images for pastes 7 and 8 taken at 3,000× magnification, and for pastes 9 and 10 at 10,000× magnification.)

heat transfer in the oven: one system involves supplying heat via infrared radiation, the other via conventional convection. Fig. 6 shows the electrical data for the solar cells prepared in this study, where the red and blue columns indicate curing by infrared radiation and by convection respectively.

The short-circuit current J_{sc} (Fig. 6(a)) for the commercial paste is of the order of 37mA/cm^2. With the infrared radiation profile, J_{sc} is around 0.1mA/cm^2 higher than with convection heating. In the case of the IKTS paste, a J_{sc} of 36.7mA/cm^2 is obtained, and the IR profile again also results in slightly higher values than with convection

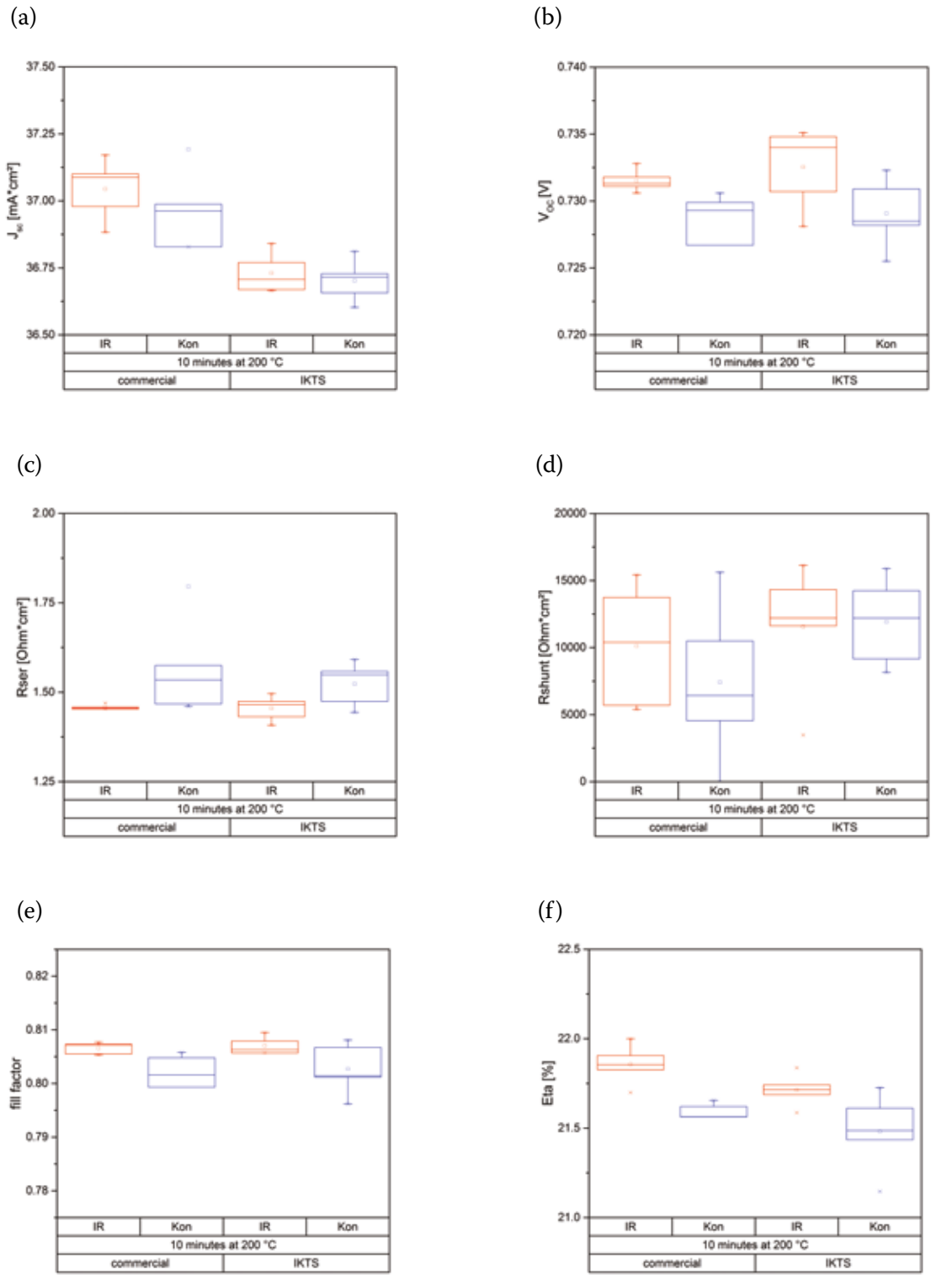

Figure 6. Electrical data for the solar cells prepared in this study as a function of the heat transfer and the paste used for printing: (a) short-circuit current J_{sc}; (b) open-circuit voltage V_{oc}; (c) series resistance R_{ser}; (d) shunt resistance R_{shunt}; (e) fill factor FF; (f) efficiency. Red columns = IR radiation; blue columns = convection. Each graph depicts the results for two pastes: commercial paste (left two columns), and IKTS paste (right two columns).

heating. A comparison of both pastes reveals that the commercial paste generates an approximately 0.25mA/cm^2 higher J_{sc} than the IKTS paste, an increase due to less spreading of the commercial paste and thus a smaller area shaded by the metallization grid.

The V_{oc} (Fig. 6(b)) for the commercial paste is ~0.73V with both curing conditions, which is comparable to that for the IKTS paste. For both pastes, the IR radiation results in a slightly higher voltage, and for the commercial paste the standard deviation is lower.

Similar results can be observed for the series resistance (Fig. 6(c)). As regards IR radiation, both pastes produce a value of R_{ser} below 1.5Ω·cm^2, with a low standard deviation; the resistance is roughly 0.1Ω·cm^2 higher using convection heating. The shunt resistance is comparable for both pastes and both curing systems.

On the basis of the data, the fill factor is greater than 80%: with the use of IR curing, a FF of 80.5% for both pastes is measured, whereas with convection heat transfer, the FF is 80.1%. The result is an efficiency level of more than 21.0%. The commercial paste yields efficiencies of 21.9% using IR curing, with a maximum cell efficiency of 22% recorded. With convection heat transfer, efficiencies of 21.6% (maximum 21.7%) are obtained. For the IKTS paste, however, the efficiency levels are somewhat lower: 21.7% efficiencies (maximum 21.8%) are achieved with IR curing, and 21.5% efficiencies (maximum 21.7%) with convection profiles. However, the use of IKTS paste offers a significant advantage with regard to handling: unlike the commercial paste, it can be stored in the fridge rather than in the freezer, which means that processing is easier because no thawing and freezing times need to be considered. Moreover, future optimization of the rheology of the paste should minimize spreading, which will result in less shading-induced J_{sc} loss.

IR curing has the advantage of moderate improvements in electrical performance. The use of radiation-based profiles results in a deeper heat transfer because of IR absorption in the wafer as well as in the silver; this means that the heat spreading in the printed layer is more homogeneous than in the case of convectional heating. With conventional heat transfer, the heat must be conducted from the surface by the metal particles to the deeper layers of the paste. This is time consuming and so the thermal budget is somewhat lower than with IR radiation; for this reason, IR is favoured for HJT cell curing.

> "The IKTS paste can be stored in a fridge instead of a freezer, which makes it a lot easier for handling by the operator."

Conclusion

In this paper an investigation of material concepts for new low-temperature contact pastes for HJT solar cell preparation has been reported. Screen-printable pastes, which are curable at 150–200°C, can be prepared using suitable polymer–solvent combinations. However, the evaporation rate and polymer cross-linking kinetics must be carefully matched. If the cross-linking occurs too fast, solvent evaporation is hindered; moreover, if fast cross-linking polymers are used, particle arrangement is inadequate, and the percolation path creation is impeded. Both of these effects lead to an increase in the resistance (R = 106.1mΩ/sq. for paste 3, compared with R > 1,000mΩ/sq. for paste 5).

If the reaction kinetics is controlled by using a suitable polymer, the resistance can be further reduced to 25.1mΩ/sq. as a result of optimized particle arrangement (paste 7). Another improvement in resistance can be obtained by means of additives, such as LMPA, or by using silver nanoparticles. The LMPA melts during curing and promotes interconnections between the silver particles; this results in decreased resistance, and lower paste costs because of the reduction in the amount of silver used.

With the use of nano silver (paste 9), an additional sintering at low temperatures can be triggered, and the resistance can be decreased to 2.7mΩ/sq. as a result of conduction through sinter necks. This is also possible by using a combination of micron-scale and nano silver powder (paste 10). Both of the nanoparticle pastes offer the second advantage of lowering the solids content, which in turn decreases the cost.

Solar cells were prepared using paste 7; with this IKTS paste, it was possible to achieve efficiencies similar to those of a state-of–the-art commercial paste. A major advantage of the IKTS paste, however, is that it can be stored in a fridge instead of a freezer, which makes it a lot easier for handling by the operator.

Finally, it was found that curing the pastes with an IR radiation profile improves electrical performance, while at the same time decreasing the standard deviation.

References

[1] SEMI PV Group Europe 2016, "International technology roadmap for photovoltaic (ITRPV): 2015 results", 7th edn (Mar.), Version 2, pp. 30–32 [http://www.itrpv.net/Reports/Downloads/].

[2] Lovinger, A.J. 1979, "Development of electrical conduction in silver-filled epoxy adhesives", *J. Adhesion,* Vol. 10, No. 1, pp. 1–15.

About the Authors

Stefan Körner is a Ph.D. student at the TU Dresden, Germany. He received his diploma in chemistry from the Chemnitz University of Technology in 2012 for research on the topic of gold nanoparticles for biochemical applications, in cooperation with the Leibniz IOM (Leipzig). He then joined the division of thick-film pastes and photovoltaics at Fraunhofer IKTS, where he works on paste development for low-temperature applications, such as HJT solar cells, and on high-temperature pastes for crystalline solar cells.

Markus Eberstein studied materials science at TU Berlin, with a particular focus on glass, and received his Ph.D. in 2001 in the field of microelectronics materials from the BAM Federal Institute for Materials Research and Testing, Berlin. He is currently the manager of the thick-film technology and photovoltaics group at Fraunhofer IKTS. The main topics of his research are structure–properties relationships of glass and ceramic thick-film materials, sintering kinetics, paste rheology and microstructure engineering.

Enquiries

Stefan Körner
Fraunhofer IKTS
Winterbergstraße 28
01277 Dresden
Germany

Tel: +49 351 2553-7817
Email: stefan.koerner@ikts.fraunhofer.de